Electric-Field Emission Mechanism in Q-Carbon Field Emitters

Ariful Haque,* Subrata Karmakar, Ravi Kumar Trivedi, Brahmananda Chakraborty, and Ravi Droopad

Read Online

ACCESS | 📊 Metrics & More | 📰 Article Recommendations

ABSTRACT: In this paper, we report the excellent field emission properties of Q-carbon and analyze its field emission characteristics through structural, morphological, and electronic property correlations, supported by density functional theory (DFT) simulation studies. The Q-carbon field emitters show impressive and stable field emission properties, such as a low turn-on electric field of ~2.38 V/μm, a high emission current density of ~33 μA/cm^2, and a critical field of ~2.44 V/μm for the transition from a linear region to the saturation region in the F−N plot. The outstanding field emission properties of Q-carbon are attributed to (i) a unique sp^2/sp^3 mixture in Q-carbon, (ii) sp^2-bonded highly conductive amorphous carbon-rich channels inside the Q-carbon cluster, (iii) a large local field enhancement due to the local geometry and microstructure of Q-carbon, and (iv) the presence of sp^2-bonded amorphous carbon regions in the composite film. The temperature-dependent field emission properties, such as extreme sensitivity and an enhancement in the emission current density with temperature, can be explained by the local density of states near the Fermi level and the excellent thermal stability of the Q-carbon field emitters. From DFT simulation studies, the computed work function and the field-enhancement factor were determined to be 3.62 eV and ~2300, respectively, which explains the excellent field emission characteristics of Q-carbon. The obtained field emission properties, in most cases, were superior to those from other carbon/diamond-based field emitters, which will open new frontiers in field emission-based electronic applications.
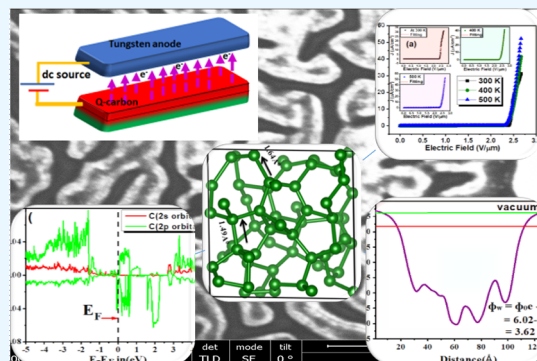
1. INTRODUCTION

Field emission from flat surfaces can demonstrate some useful and desirable characteristics, such as high brightness, fast response, extremely high resolution, and small energy consumption, which make the emitters suitable to fabricate vacuum-fluorescence display panels, fast-response switching devices, frictionless motors, and so on.[1] Carbon-based field emitters are desirable because the material can sustain a high electric field and breakdown occurs at exceptionally large fields, of the order 800−1000 V/μm.[2] Other widely used materials, i.e., Si, GaAs, and SiC can sustain only up to 30, 40, and 300 V/μm, respectively.[3] However, different carbon-based field emitters have different limitations from the viewpoint of growth, field emission current density, stability, and device processing. For example, carbon nanotubes (CNTs), one of the most explored carbon-based field emitters, tend to burn out in a way that the tallest CNT in the emitting zone first experiences the highest field and therefore emits most of the current. Subsequently, the emission occurs from the next tallest CNT, which survives for a time and then also burns out. Thus, all CNTs burn out one after another until emission ceases completely.[4] Nonetheless, CNTs can so far only be formed by plasma deposition,[5,6] chemical vapor deposition,[7] or extracting from a post-discharge deposit[8] at high temperatures, usually over 700 °C. Moreover, CNT film emitters usually exhibit very

different field emission (FE) properties, even if they are produced by the same procedure.[9] On the other hand, electron emissions were observed only from the edges and corners of individual single- and multi-layer graphene, which is unsuitable for practical applications.[10] Although the negative electron affinity (NEA) of diamond is favorable for desirable FE characteristics, attempts to utilize the NEA did not quite lead to the fabrication of diamond-based practical FE devices due to the wide bandgap and poor conductivity of pristine diamond.[11] Recently, various laser processing techniques have been discovered to grow various metastable forms of carbon with hierarchical structural morphologies.[12−14] Moreover, complex and expensive microfabrication and processing techniques, such as patterning and/or etching of diamonds to give suitable pyramid or needle shapes, are usually required to obtain a large field-enhancement factor in diamonds.[4] The use of diamond-like carbon (DLC) films as a cold cathode material is also limited owing to their low FE current density and high

threshold fields.[15] Nonetheless, the carbon-based conjugated polymer (poly 3-octyl-thiophene) films have demonstrated a very low turn-on field and good current density, but the current density drops to 55% of its initial value in 2 h which makes this material incompetent for practical applications.[16]

Field-emission efficiency of an emitting material depends upon a combination of factors which includes the conductivity of the emitter, mechanical and electrical stability under large electric fields, the surface work function, and the resistance of the emitter/substrate interface.[17] An ideal field emitter should be a good electrical conductor with a low work function and a high enhancement factor and be stable at high emission current densities. Our investigations show that Q-carbon possesses all these properties. In addition to that, Q-carbon is considered a strong candidate for field-emission cathode devices because of its low electron affinity and chemical inertness.[18] Furthermore, due to its excellent physical properties, such as high hardness, good thermal conductivity, and good mechanical, chemical, and thermal stability, there is considerable interest in the use of Q-carbon as a cold cathode material for the fabrication of high-performance electronic devices that could be used in high-temperature and heavy radiation environments. The inertness prevents the Q-carbon surface from aging, a process often observed in field-emission studies of metals. This property is fundamentally important for the stabilization of field-emission cathodes, providing reliability and durability. Recently, Zaria *et al.* grew ultra-nanocrystalline diamond (UNCD)/hydrogenated amorphous carbon (a-C:H) composite films by coaxial arc plasma deposition and observed that the presence of sp^2-grain boundaries (GBs) in nano-sized-sp^3 diamond grains enhanced the electrical conductivity significantly.[19,20] Therefore, the suitable microstructure, ideal sp^2/sp^3 carbon ratio in the nano-composite Q-carbon films, and highly packed diamond tetrahedra in the Q-carbon structure are some of the attractive features of the superior FE properties. To determine the electronic structure of atoms, molecules, and solids, physicists and chemists have employed the density functional theory (DFT) quantum-mechanical (QM) technique since the 1970s, and it has gained a lot of attention nowadays in computational solid-state physics. Computing observables that are directly related to experiments are the basis of a DFT study with QM approaches. In addition to the primary quantities, such as energies, structures, and spectroscopic properties, the DFT study also helps us to identify the electronic, magnetic resonance, and vibrational spectroscopic characteristics where theory and experiment can collaborate and complement one another.[21]

In this study, we have investigated the fabrication and characterization of high-performance Q-carbon field emitters with excellent emission properties. The mechanism of the excellent FE properties of Q-carbon has been illustrated through the structural-property correlations. To develop a better understanding, we have also made a comparative investigation of field emission properties in Q-carbon with other carbon and non-carbon-based conventional field emitters. Here, the DFT study was performed to observe the total density of states (TDOS) and partial density of states (PDOS) and to determine the work function of the Q-carbon field emitter after structural optimization. The observed field emission characteristics suggest that this nanostructured thin film can be a prospective material for next-generation flat panel display applications.

2. EXPERIMENTAL SECTION

2.1. Fabrication of Q-Carbon Nano-Composite Film. A compact and high-quality graphite target (99.99% pure) was placed on a rotating target holder inside the pulsed laser deposition (PLD) chamber for the deposition of amorphous carbon films on crystalline sapphire substrates. The separation between the target and the substrate was ~4 cm. A krypton fluoride (KrF) pulsed excimer laser with 248 nm wavelength, 20 ns pulse duration, 5 Hz rep-rate, and an energy density of ~3 J/cm² was used for the deposition. A pressure of ~1 × 10⁻⁶ Torr was maintained throughout the deposition inside the stainless steel PLD chamber. We have systematically varied the laser parameters, such as the laser energy density, to optimize the deposition conditions of the amorphous carbon thin film on the r-sapphire substrate. An argon fluoride (ArF) pulsed excimer laser with 193 nm wavelength and 20 ns pulse duration was used to irradiate the amorphous carbon film to form a Q-carbon thin film. An energy density of 0.6 to 0.7 J/cm² was maintained to create the molten state of carbon which is successively quenched into a super undercooled state from Q-carbon within a very short time (<250 ns). Raman spectra were collected by Horiba LabRAM HR Evolution Raman technology from 900 to 2300 cm⁻¹ using a 532 nm laser excitation wavelength.

2.2. Characterization and FE Test. We have performed Raman spectroscopy to characterize the nanostructure of the films. Unpolarized Raman spectra were recorded *ex situ* at room temperature in a backscattering geometry for 532.16 nm excitation using a WITec confocal Raman microscope system (alpha 300 M) coupled with a notch filter and an insulating spacing plate of 100 μm thickness. The morphologies of our samples were characterized by a high-resolution FEI Verios 460 L scanning electron microscope. Field-emission tests were carried out in the parallel plate diode configuration with an anode of tungsten sheet, and a Q-carbon nano-composite thin film acted as a cathode, maintaining pressure below 5 × 10⁻⁷ Torr in an ultrahigh vacuum chamber. No forming process was needed to obtain emissions from these films. No macroscopic surface damage was observed on the films after the emission testing, which is expected owing to the robust property and moderate conductivity of the Q-carbon composite films. All electrical measurements were taken after waiting for the electrostatic equilibrium to be reached. The measurements were performed in the dc mode.

2.3. Computational Details. We have performed geometry optimization and energy calculations within the context of DFT by using the projector augmented wave (PAW) method along with the generalized gradient approximation (GGA) functional as implemented in VASP (Vienna ab initio simulation package).[22−25] The amorphous form of Q-Carbon, consisting of 64 carbon atoms, was considered for initial structural relaxation, and it was carried out till the force on an individual atom became less than 0.01 eV/Å, and the plane wave cut-off energy was taken as 550 eV. A Monkhorst-Pack[26] grid of 7 × 7 × 1 K-points was used for relaxation, and we used 9 × 9 × 1 K-points to analyze the DOS.

3. EXPERIMENTAL RESULTS AND DISCUSSION

3.1. Surface Morphological Analysis. Figure 1a shows the high-resolution and large-area SEM image of the Q-carbon nano-composite film, where the bright regions refer to the Q-carbon structures and the rest dark region is the amorphous
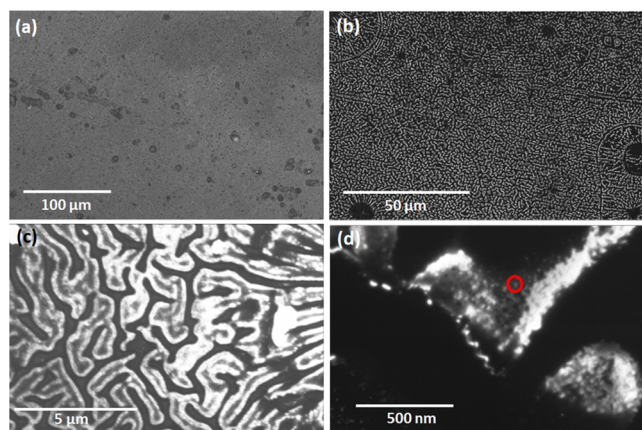
Figure 1. High-resolution SEM image of the Q-carbon nano-composite film at (a) 100 μm scale and (b) 50 μm scale, showing uniformly distributed sp³-rich Q-carbon regions (bright) in the sp²-rich highly conductive amorphous carbon (dark). (c) Broad curvy Q-carbon region at a higher magnification with a scale of 5 μm. (d) Magnified view of the Q-carbon clusters in which individual Q-carbon grains can be observed (inside the red circle). The amorphous carbon channels in between the Q-carbon grains inside the cluster are also evident.

Figure 2. Raman spectrum of Q-carbon (dark yellow) and amorphous carbon region (black) in the region from 900 to 2200 cm⁻¹.

carbon. The Q-carbon clusters were found to grow uniformly throughout the nano-composite film, and they are isolated from each other by an intermediate sp²-rich amorphous carbon region. It is also evident from this image that all Q-carbon clusters have similar dimensions and regular shapes throughout the film. Figure 1b is a high-magnification SEM image showing the emitter surface condition. Each of the Q-carbon cluster is formed by multiple Q-carbon grains (elucidated inside the circular red line) which can be seen in this image. The unconverted sp² carbon-rich amorphous carbon forms the channel between these grains. The electron-emitting channel for enhanced field emission is shown in Figure 1c at a higher magnification scale where the broad whitish region is Q-carbon which is surrounded by a blackish amorphous carbon region. The Q-carbon nanocluster is surrounded by thin boundaries that are rich in sp² bonds, and one small Q-carbon cluster region is shown in Figure 1d marked by a red circle. Due to the high conductivity of these boundaries, the flow of electrons is enhanced through each Q-carbon nanocluster, and it serves as a cathode. It is hypothesized that an effective FE device is produced by the high density of grain boundaries within the Q-carbon clusters connected to the amorphous carbon matrix.

3.2. Raman Spectra Analysis. The Q-carbon nano-composite films were characterized by Raman spectroscopy to identify different sp³/sp² bonding characteristics at different regions of the field emitter. Figure 2 shows the micro-Raman spectrum of the Q-carbon region where the D and G bands are observed at 1345 and 1568 cm⁻¹, respectively.[18,27] Another very small hump/shoulder peak at 1620 cm⁻¹ arises due to a disorder-induced breakdown of the Raman selection rule. The sp³ carbon content was determined to be more than 76%, which compares with the previous studies.[18,27] The amorphous carbon region, illustrated by the black spectrum in Figure 2, is characterized by a very broad Raman band centered around 1400−1600 cm⁻¹. The exact shape and position of this band depend on the bonding characteristics and the percentage of the sp²/sp³ content. The fitting profile of this amorphous carbon region shows an sp³ content of around 35%, and the
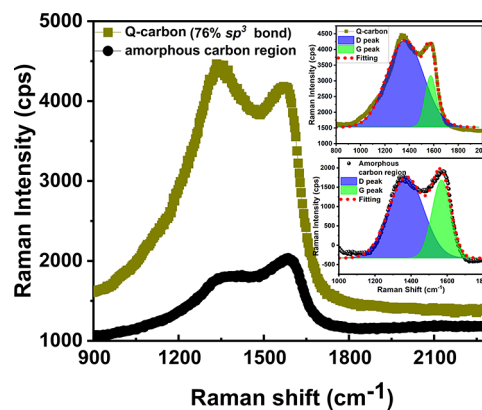
remaining 65% is sp² carbon, which provides the conductivity in the field emitter. No Raman peak at ~2160 cm⁻¹ is observed, indicating the absence of any sp¹-bonded sites.

3.3. Field Emission Measurements. Figure 3a represents the field-emission characteristics of Q-carbon nano-composite films at different temperatures. All emission current density versus applied electric field (J−E) plots during the field emission measurements show an exponential behavior above the turn-on electric field (E_{TO}), which is defined as the required electric field to obtain a current density of 1 μA cm⁻². The E_{TO} of the FE curve at room temperature is found to be ~2.38 V/μm. We observe a decrease in the E_{TO} with increasing temperature. This could be due to the modification in the electronic structures, such as the activation of acceptor-like levels or impurity levels at elevated temperature regions. This high-temperature condition may also facilitate the transportation of electrons through the field emitter. Additionally, the interband states might get activated at high temperatures and electrons from these states could reach the anode directly under the applied electric field. All FE curves fitted well with the Fowler-Nordheim (F−N) relationship which can be expressed by eq 1. The F−N plots are shown in Figure 3b according to

$$J = A\left(\frac{\beta^2 E^2}{\varphi}\right) \exp\left(-\frac{B\varphi^{3/2}}{\beta E}\right) \exp\left(-\frac{\Delta W^{\text{S}} - \Delta W^{\text{P}}}{2k_{\text{B}}T}\right) \quad (1)$$

where J represents the field emission current density, E represents the applied electric field between the tungsten anode and Q-carbon cold cathode emitter (E is the ratio between the applied voltage V and the distance between the metal anode and the field emitter plane, d), φ represents the work function, β represents the field-enhancement factor, T is the absolute temperature, and k represents the Boltzmann constant. The surface potential barrier for sp³-bonded nanostructures due to surface states is represented by ΔW^{S}, and the decrease of the surface potential barrier due to field penetration is expressed by ΔW^{P}. The two well-known constants A and B have the values $A = 1.54 \times 10^{-6}$ A eV V⁻² and $B = 6.83 \times 10^3$ eV⁻³/² V⁻¹ μm. Our results followed the F−N equation at the low field. However, at the high-field region, after a critical electric field, the J−E plots deviated from the linear F−N relationship, which was due to the current saturation of the Q-carbon field emitters at high applied electric fields. Similar characteristics of F−N plots in the high-field regions have been reported in the earlier studies on
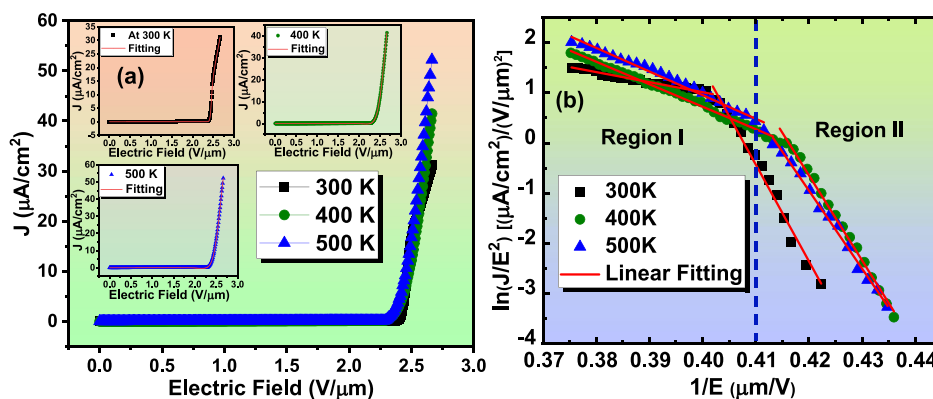
Figure 3. Field emission measurements from the Q-carbon nano-composite cathode film at different temperatures. (a) $J-E$ plots in the temperature range from 300 to 500 K. (b) F−N plots of corresponding $J-E$ data show two distinct slopes at high and low electric field regions.

graphene,[28] diamond,[29] and carbon nanotubes.[30] As expressed in the F−N equation, the emission current density of an emitter exponentially depends on the field-enhancement factor, which is an intrinsic material property. In the present study, we have determined the field-enhancement factors from the slope of the F−N plots (straight line behavior in the low field region), which is mathematically expressed as

$$\beta = -\frac{(6.83 \times 10^3)}{slope}\varphi^{3/2} \qquad (2)$$

The work function of Q-carbon was calculated as 3.62 eV from the DFT simulation; the low-field β was found to be 2300 at room temperature, which is higher than most of the carbon and non-carbon-based conventional field emitters. The calculated β values of the Q-carbon field emitter at different temperatures are tabulated in Table 1. Less turn-on or

Table 1. Field Emission Characteristics of Q-Carbon Field Emitters in the Temperature Range from 300 to 500 K

operation temperature (K)	turn-on field (V/μm)	maximum current density (μA/cm^2)	$\beta 1$ (region I)	$\beta 2$ (region-II)
300	2.38	31.62	2300	241
400	2.35	42.90	1058	280
500	2.32	53.10	1113	305

threshold field and high field emission current density of the Q-carbon field emitters are reported in in this study compared to those for the as-deposited DLC film, which exhibits the great impact of the laser annealing process on the DLC thin film.[31−33]

3.4. Field Emission Mechanism in Q-Carbon. Field-emission characteristics of an emitter are governed by a combination of factors which includes the conductivity of the emitters, the surface work function, the morphology of the film, and the relative sp^3/sp^2 ratio. An ideal field emitter should be a good electrical conductor having a low work function, a high field-enhancement factor, and good stability at high emission current densities. The Q-carbon nano-composite films have excellent conductivity and a robust structure with a low work function, which is promising to construct some excellent field-emission devices. It shows a very high field-enhancement factor due to several reasons which will be explained below. Q-carbon consists of numerous highly packed sp^3-bonded diamond tetrahedra in a random order.[18] The sp^2-

bonded carbon atoms remain in between these diamond tetrahedra to provide the necessary conduction for the electrons during the FE measurements. The sp^2 carbon shows high electrical conductivity that has a better ability to provide large FE current densities.[34] This sp^2-carbon also causes electron delocalization and improves electron hopping between the sp^3-rich Q-carbon grains resulting in further accelerated electron transportation in the Q-carbon nano-composite structures.[33,35] As the sp^3-rich Q-carbon grains possess very low/negative electron affinity, the electrons can be easily extracted from the Q-carbon surface in the presence of an applied external electric field.[27] Thus, electrons can be launched into a vacuum from Q-carbon, which are supplied by the sp^2 carbon-rich amorphous carbon channel under the action of an external electric field. Although sp^2-bonded carbon provides tremendous advantages for the improved FE characteristics in carbon-based structures, a large amount of sp^2-carbon in the emitting structure is undesirable owing to the fact that negative electron affinity is involved with the sp^3-content and an excessive amount of sp^2-carbon in the emission sites is responsible for the increase in the electron affinity.[36−38] The laser annealed Q-carbon is formed by the liquid phase quenching of the carbon melt during the nanosecond laser irradiation on the PLD-grown carbon films. The high packing efficiency (80%) and the uniform distribution of a suitable fraction of sp^2-bonded C throughout the sp^3-bonded matrix in Q-carbon provide an ideal platform for enhanced field emission.[27]

Combining the Raman analysis and results of the FE measurements, the outstanding FE characteristics of the Q-carbon composite structure can be explained by the micro-structure and the bonding characteristics of the atoms present in the Q-carbon structure. The emission current is significantly high, and the turn-on field is very low for Q-carbon composite films. We envisaged these outstanding FE properties from the following factors: (i) defect-induced bands owing to sp^2 content. The defect-induced energy bands created by sp^2-bonded atoms are responsible for the enhancement in FE current density. Defect-induced energy bands can be induced throughout the energy gap of sp^3-rich Q-carbon due to the presence of structural defects created by the sp^2-bonded carbon. The formation of these defect bands raises the Fermi level toward the conduction band and thus reduces the work function for the field emission which is further supported by the DFT analysis discussed in the Simulation Results and Discussion section of this article. Thereby, the surface potential

Table 2. Comparison of the FE Properties with Conventional Non-Carbon-based Field Emitters

field emitters	turn-on field (V/μm)	threshold field (V/μm)	field-enhancement factor (β)	ref	year
Q-carbon	2.4 (1 μA/cm^2)	2.65 (30 μA/cm^2)	2300	current study	2022
ZnO nanosheets arrays	2.4 (0.1 μA/cm^2)	6.4 (50.1 μA/cm^2)	5812	46	2014
Si nanowires	2 (10 μA/cm^2)	3.4 (1 mA/cm^2)		47	2006
WS$_2$ nanotube		1.5 (1 μA/cm^2)	3526	48	2014
GaN nanowires	9.1 (0.1 mA/cm^2)		730	49	2011
TiO$_2$ nanotube arrays	2.8 (1 μA/cm^2)	8.0 (0.15 mA/cm^2)	5580	50	2006

Table 3. Comparison of the FE Properties with Different Carbon-based Field Emitters

field emitters	turn-on field (V/μm)	threshold field (V/μm)	field-enhancement factor (β)	ref	year
Q-carbon	2.4 (1 μA/cm^2)	2.65 (30 μA/cm^2)	2300	this study	2022
single-crystal diamond	4.27 (0.1 μA/cm^2)	7.6 (113.2 μA/cm^2)	1000	51, 52	2003 & 1996
nano-diamond films	2.2 (1 μA/cm^2)	6.4 (0.72 mA/cm^2)		53	2003
N-doped nano-diamond	3 (1 nA)			54	2009
graphene nanosheet array	2.6 (10 μA/cm^2)	5.8 (1 mA/cm^2)	3788	55	2012
freestanding graphene-diamond	2.2 (0.1 mA)	4.8 (0.6 μA)	1950−4720	56	2011
DLC/Si	5.6 (0.01 μA/cm^2)	14.3 (15.2 μA/cm^2)		15	2000
patterned DLC/Ti/Si	2.1 (0.01 μA/cm^2)	14.3 (1.23 mA/cm^2)		15	2000
CNT arrays	3.22 (10 nA)		1900−2500	57	2006
carbon nanowalls	4.7 (0. 1 mA/cm^2)	6 (1 mA/cm^2)	1399	58	2015
vertically aligned CNT/DLC	2.0 (undefined)	2.1 (10 μA/cm^2)	2529	4	2013

barrier height of Q-carbon is reduced compared to that of the other carbon-based materials, such as diamond or DLC, and the electron emits easily from the Q-carbon surface.[39] The sp^2-carbon-induced spatially localized states also enable hopping conduction in the Q-carbon structure.[40,41] The observed increase in the current density with temperature under a constant applied electric field is also attributed to the smaller energy separation among the defect bands in the bandgap associated with the sp^2 carbon in the Q-carbon structure. Moreover, the lowering of E_{TO} with temperature is a direct consequence of decreasing effective potential barrier height for electron emission which was discussed elaborately in our previous papers.[27,42] Thus, the combination of the reduction of E_{TO} and enhancement of the emission current with temperature is observed due to the higher probability of electron injection into the electron bands during the transport process, originating from the defect state-induced decrease in the effective potential barrier height for field emission. (ii) Increase in field-enhancement factor owing to sp^2-sp^3-sp^2 (MIM) microstructures. This hypothesis for the novel Q-carbon structure proposes that the sp^2-rich conducting grain boundary surrounding the individual Q-carbon grain in a Q-carbon cluster forms cascaded MIM microstructures, which results in obtaining an enhanced β. The β is the ability of an emitter surface to enhance the local electric field at the emission spots, which is defined as the ratio of the local electric field to the macroscopic electric field. Assuming a parallel configuration of semi-infinite electrode plates, the local electric field (E_{local}) in the emitting Q-carbon entities is given by the following expression

$$E_{local} = \beta \frac{V}{d} = \beta E \qquad (3)$$

The β can be affected in different ways, such as geometrical parameters of the FE device structure, morphology of emitters, and the distribution of different bonding characteristics in the emitter.[43] The structural inhomogeneity in the Q-carbon nano-composite films is created due to the distribution of the sp^2

carbon in the sp^3 matrix. Under the applied electric field, the abrupt termination of the field lines occurs at the non-conducting zones due to the inhomogeneity of the structure which amplifies the β.[44] Hence, the sp^2/sp^3/sp^2 entities should constitute the preferential sites for electron emission due to the activation of this junction at a low applied electric field. Unlike the case of the F−N theory for pure metals, the dependence of the field-enhancement factor in a sp^2/sp^3 system cannot be elucidated solely by geometric features. In the Q-carbon structure, it mainly depends on the combination of electronic and dielectric properties of highly packed sp^3 and sp^2 nanophases at the atomic level. The distribution of sp^2 carbon in a sp^3 matrix creates a dielectric inhomogeneity, which also enhances the field-enhancement factor.[45] This could be attributed as one of the main reasons for the observed high field-enhancement factor in the Q-carbon field emitters. The F−N theory is useful to compare the FE performance of Q-carbon thin films with other carbon- and diamond-based nanostructures and films whose FE characteristics were analyzed within the F−N framework. Following this, the field-enhancement factors obtained from Q-carbon are compared and tabulated in Tables 2 and 3 with other non-carbon and carbon-based field emitters, respectively. Two regimes were inferred from the F−N linearization of the J−E data; each corresponds to a distinct field-enhancement factor, β1 (from ∼2300 to ∼1113) at the low-field and β2 (from ∼241 to ∼305) at the high-field regions. After field intensification, a local field of ∼7050 V/μm could be attained (eq 3) by an applied macroscopic activation field of 2.4 V/μm at room temperature.

(iii) Finally, the conductivity phenomena and the FE property in the Q-carbon nano-composite structure comply with the Latham's unifying theory[29,59] which explains/correlates the critical role of the embedded nanosized conducting channels in a nonconducting nanostructured matrix, and the spatially localized electronic states occurring in parallel to the FE mechanism. In the Q-carbon nanostructure, the sp^2-rich amorphous carbon-rich conducting

channels are embedded in the sp^3-rich relatively less conducting Q-carbon grains. This amorphous carbon region is like a semimetal (free electron density ~10^{18} cm^{-3}) which supplies the free electrons. On the other hand, unlike diamond, the partial overlapping of π electron orbitals from the small sp^2-bonded carbon fraction occurs in Q-carbon, which also helps electrons to reach the top of the Q-carbon surface within a Q-carbon grain during the emission process. The rest of the three valance electrons lying in a plane form strong σ bonds, which coincide with the basal plane. The electronic levels lying near the Fermi level are formed due to the weak π bonds, whereas the σ bonds are responsible for the electronic bands far from the Fermi level. The formation of these bands is depicted schematically in Figure 4a in the form of the electron DOS.
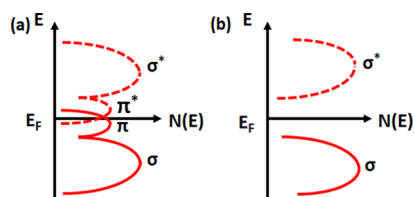

Figure 4. (a) Schematic representation of the electronic DOS, $N(E)$, of Q-carbon which consists of a small percentage of sp^2 carbon and (b) similar diagram assuming no sp^2 carbon in between the sp^3-bonded diamond tetrahedra in the Q-carbon structure. The π and $\pi*$ states near the Fermi level arise due to the sp^2 carbon.

Such arguments are only valid for carbon atoms surrounded by the same atoms on all sides. The corresponding hypothetical electronic DOS is shown schematically in Figure 4b if there were no sp^2 carbon atoms present in the Q-carbon structure.

Electrons must have enough energy to cross the potential barrier at the metal-vacuum interface or the potential difference between the Fermi level of the metal and the vacuum to depart from a metal surface. The electron potential energy as a function of x from the metal-vacuum contact for Q-carbon is shown in Figure 5a. The electric field and the image force, which add to the position-dependent factors $-eEx$ and $\frac{e^2}{4x}$, respectively, make the barrier thin and reduce the barrier height for electron field emission. When an electric field E is applied perpendicular to the emitting surface, the effective potential on an electron at a distance x from the surface is also shown in Figure 5a. The potential barrier is altered by the

applied electric field E, becoming thinner (triangular), and the effective barrier height is decreased. The electrical conductivity of the amorphous carbon region of the film is close to metallic (clearly seen from the DFT results), which allows the flow of a high current density. Under the presence of an applied electric field, the electrons tunnel through the thin energy barrier at the interface of the two carbon phases and leave the Q-carbon surface due to its favorable low electron affinity, which has been shown in Figure 5b. The density of the unpaired electron states near the Fermi level is high in the Q-carbon region;[60] consequently, the wave-function overlap takes place, which results in electron delocalization.[61,62] Under an applied electric field, the degree of field penetration into a semiconductor depends on the conductivity of the sample. As a result, we can infer an immediate link between the emission mechanism and the extent of field penetration. The extent of the field penetration due to the externally applied electric field decreases with increasing conductivity. The field lines from the anode terminate on the amorphous carbon region in the Q-carbon nano-composite film because of the high electrical conductivity of this region, owing to the high fraction of sp^2 carbon. On the other hand, there are some field penetrations associated with the Q-carbon region, and the emission is controlled by the properties at or near the front of the film-vacuum interface, which is referred to as the "front surface"-controlled FE mechanism. A schematic of the field emission from the Q-carbon cathode surface to the tungsten anode under a dc field is shown in Figure 5c.

Altogether the microstructural heterogeneity, uniform distribution of the sp^2 carbon at the atomic level, and hence the modification of the electronic structure with the sp^2-rich carbon are envisaged to play key roles in obtaining excellent FE properties. Application of an external electric field results in the extraction of electrons from the Q-carbon film surface. Replenishment of the emitted electrons to the Q-carbon region is accomplished by the conductive channels around the Q-carbon grains. Such a process helps us to explain the non-uniform nature of the emission across the surface of the film (on the nano- to microscale) in which the local arrangement of the bonding characteristics of the carbon atoms is important. In Q-carbon nano-composite films, with inhomogeneous structural and electrical properties, the percentage of the conductive zones and the sp^3/sp^2 ratio can be tailored to control the charge transport by tuning the laser energy density and the rate of undercooling during the ultrafast melting and
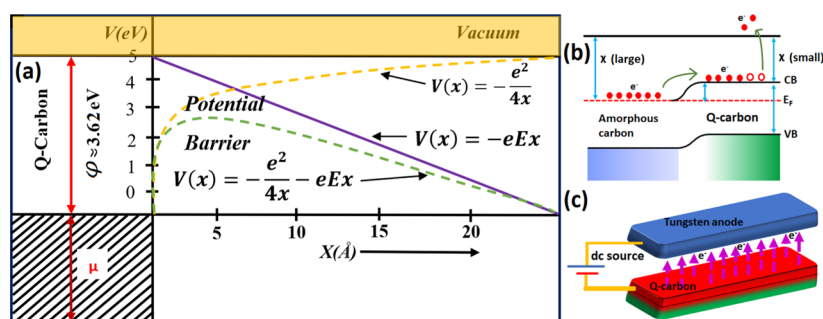

Figure 5. (a) Potential energy as a function of distance x (Å) for field emission in Q-carbon. (b) Illustration of the field electron emission from the relative band diagram perspective (the diagram does not present the original values of the respective phases of carbon). The small height between the top of the conduction band (CB) and the vacuum level is due to the extremely low electron affinity which makes it easier for the electrons to reach the vacuum level under the applied electric field. (c) Schematic illustration of the electron emission from the front surface of the Q-carbon thin film (cathode) to the tungsten anode under an external dc field.

Table 4. Origin of Electric Field Emission, Transport, and Its Mechanism from a Variety of Cathodes[70]

compounds	source of field emission	transport mechanism	electron emission mechanism
any flat metal surface	high DOS at Fermi surface (EF)		follows the Fowler-Nordheim (FN) model for work function (4–5 eV) ($\beta = 1$)
any Spindt-tip like structures	high DOS at Fermi surface (E_F)		follows the Fowler-Nordheim (FN) model for work function (4–5 eV) and ($\beta > 50$–100)
any wide gap semiconductor or insulator, *i.e.*, diamond, AlN	substrate surface	transport occurs *via* conduction band or defect level present	follows the NEA and Fowler-Nordheim model
DLC	substrate surface	hopping mechanism	follows the FN model with negligible field penetration
polymer-like amorphous carbon	substrate surface	effects from space charge	follows the FN model with important field penetration
CNTs	substrate surface	transport occurs *via* the tube	follows the FN model for work function (4–5 eV) ($\beta > 200$) aspect ratio
CNT–polymer nano composites	substrate surface and CNT	percolation mechanism	electron transport and FN model
Q-carbon	high DOS at EF and front-surface-based emission	defect level hopping and conduction band	NEA + FN with very high β + field penetration important

quenching of the amorphous carbon by PLA. This will help us to control the field emission properties of Q-carbon nano-composite films. Unlike a-C films, which require a conditioning process before the emission of electrons from their surfaces, the Q-carbon nano-composite films show very stable J–E characteristics without any pretreatment during the FE measurements.[60] Furthermore, Q-carbon does not show any irreversible hysteresis which is a characteristic feature of some conventional carbon-based field emitters.[60] The hysteresis phenomenon is often evidenced by the successively decreasing threshold fields which reach a minimum value after several operational cycles in those carbon-based materials. Moreover, the presence of adsorbents and/or organic entities is usually responsible for the noise and flickering in the emission current and a relatively low threshold field, which are often observed at the initial state during measurements in the carbon-based field emitters. However, the stable J–E plots and the observed reproducibility with little or no fluctuations eliminate the presence of a significant amount of adsorbates in the Q-carbon nano-composite films. Therefore, Joule heating of the Q-carbon nano-composite films is not required before the FE measurements. On the contrary, different types of gases or organic species are present at the surface of hollow/tubular CNT-based field emitters, which create nano protrusions/ regions of reduced work function zones and thereby increase the field-enhancement factor.[63,64] Thus, the FE begins at lower electric fields at these nano protrusions. The formation and Joule heating-driven surface diffusion of the nano protrusions are responsible for the change in the local work function and thereby can yield instabilities in the FE current density during the FE measurements. At a large applied electric field, the local temperature becomes high due to the high current density current flow which leads to the evaporation of some adsorbates, thereby causing a drop in the FE current density. No such phenomenon occurs in the Q-carbon nano-composite films owing to the compact structure and inertness of the film as it is formed by the quenching of the molten state of carbon within a very short time (<250 ns).[18] The temperature-dependent sensitivity of the FE properties of Q-carbon indicates that several of the interband defect levels near the conduction band participate in the emission process, although the greater part of the emission current comes from the occupied states with a large DOS. This is partly responsible for the good emission characteristics. Moreover, the sp³-rich Q-carbon grains with high thermal conductivity can dissipate the produced heat to the surrounding in a very effective way

during the FE operation and help to maintain an efficient electron field emission process.

Three fundamental factors are important to understand the controlling phenomena for the field electron emission from an emitter surface: (i) the emission process from the surface to the vacuum, (ii) the source of the electrons, and (iii) the electron transport mechanism through the film.[65] We have discussed these factors for the Q-carbon nano-composite field emitters in this study and summarized and compared our findings with other extensively studied field emitting materials in Table 4. Examining the recent works on FE characteristics on carbon-based materials, researchers have demonstrated the lowest E_{TO} as 3.22 V/μm in the multi-walled CNT (MWCNT) samples.[57] On the other hand, the complex graphene-diamond hybrid film demonstrated a low E_{TO} value of 2.4 V/μm.[56] In a complex and unconventional carbon nanowall structure, researchers have obtained a low E_{TO} of ~3 V/μm.[66] Moreover, other researchers have realized an E_{TO} of ~3 V/μm in nanocrystalline diamonds.[54] Tables 2 and 3 summarize some of the important FE properties of different carbon and non-carbon-based field emitters, respectively. In the current study, the value of E_{TO} (~2.38 V/μm) for Q-carbon field emitters seems to be very encouraging. Although some of the field-emission properties of Q-carbon films are not better than those of carbon nanotubes, nanodiamonds, and graphene, the outstanding FE characteristics as a whole meet all prerequisite factors for practical applications. The Q-carbon nano-composite films can be deposited with a high deposition rate at room temperature over a large area. This is necessary for fabricating large-area flat-panel displays for commercial purposes. Moreover, the lack of adequate control capabilities on the structural, electronic, and other properties of different carbon-based films makes it difficult for practical applications. Nonetheless, cold cathodes based on Q-carbon nano-composite structures offer immense potential since it is possible to deposit the Q-carbon thin films over large areas at a very low cost. The softening temperature of most of the common display glasses is around 400 °C. The deposition temperature of most of the carbon-based field emitters significantly exceeds this temperature; thus, these materials are not compatible with the current technology. The low-temperature and controlled synthesis of Q-carbon make it a promising cathode material. Unlike most of the other emissive carbon films, the present Q-carbon nano-composite films can be deposited onto transparent and flexible polymer substrates. In addition to that, since a reliable fabrication method of diamond microtip arrays over a large area is very difficult,

nano-composite Q-carbon films with a low electron affinity could be a viable solution to produce FE displays. The low threshold field, good current stability, and low-temperature processing make these novel nanostructured carbon films very suitable for display applications. Similar FE characteristics due to the low electron affinity, wide bandgap, and excellent transport properties were recently obtained from polymer films,[16] but it is evident that emission from Q-carbon composite structures with two different carbon phases shows better long-term stability which is a prerequisite for FE-based nano- and microelectronic device applications. Although a comprehensive and well-accepted emission mechanism of carbon-based materials is not yet established,[67] these experimental results suggest that better field emission comes from more complex forms of carbon with both sp^3 and sp^2 bonds and often having heterogeneous structures at the nanoscale/atomic level.[68] The source of the large field-enhancement factors observed for different forms of carbon is still under debate.[67,69] Nevertheless, we explicitly explained the source of the large field-enhancement factor using the structural and bonding, electrical, and morphological characterizations of the composite film at the nanoscale level. The characterization and analysis in this study describe the unique origin of the extremely low-threshold electron emission from Q-carbon which is supported by the theoretical investigations described below. In addition, the emission current from this exciting material exhibits a stable emission current intensity profile with a remarkably long lifetime, two factors vital for next-generation vacuum nanoelectronics devices.

4. SIMULATION RESULTS AND DISCUSSION

4.1. Structural and Density of States Study. In the simulation study, we generated an amorphous form of the Q-carbon bulk structure and allowed it to relax and optimize. The relaxed geometry of the Q-carbon used for further studies is demonstrated in Figure 6a. The unit cell structure of Q-carbon
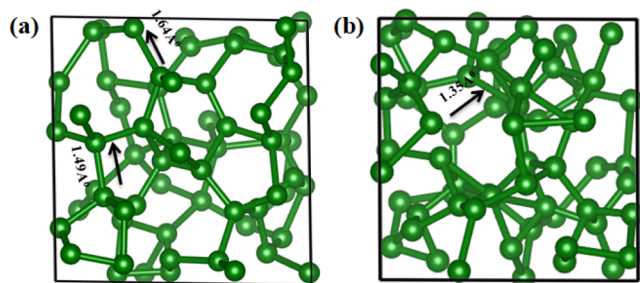

Figure 6. DFT-optimized minimum energy structure of (a) bulk Q-carbon and (b) Q-carbon layer. The arrow is indicating the bond distance between two carbon atoms. [green color balls represent C atoms].

presented in this figure is the lowest energy structure among different structures, and the coexistence of 4-fold-(sp^3) and 3-fold-(sp^2) coordinate atoms is shown by a green ball-and-stick model. This structure comprises ∼80% (52 atoms of 64 atoms) of the 4-fold coordinated carbon atoms (sp^3), and the rest 12 atoms are 3-fold coordinated (sp^2) (we used 1.64 Å and 1.49 Å as the criterion for the coordination).[71] This value is close to the experimentally observed high sp^3 ratio of ∼75−85% in Q-carbon.[72] The lattice constants of the unit cell of Q-carbon have been taken as $a = b = 7.21$ Å.[71] The Q-carbon layered

structure is also optimized and displayed in Figure 6b for local work function calculation.

4.2. Charge Transfer and Orbital Interactions. To get insights into the orbital−orbital interaction, the TDOS and the PDOS analyses have been performed for Q-carbon, and the results are demonstrated in Figure 7a,b, respectively. As we can see in Figure 7a, there are charge states on the Fermi level which shows the metallic characteristics of Q-Carbon, which was predicted previously.[71] Non-symmetric behavior of spin-up and spin-down charge states implies the magnetic behavior of Q-carbon. It can also be seen from the PDOS plot in Figure 7b that the charge states near the Fermi level are mainly contributed by the 2p orbital of carbon atoms which complies well with the recent investigation.[72] Several localized states near the Fermi level are obtained for Q-carbon from the PDOS graphs. Particularly when the 3-fold coordinated atom is surrounded by 4-fold coordinated atoms, the p$_z$-orbital of 3-fold coordinated carbon atoms in amorphous carbon cannot form a continuous Π-network as in graphite. Localized states are created in the near-gap region when 3- and 4-fold atoms are close together. A 3-fold carbon atom can be viewed as a flaw in a 4-fold-dominated carbon system even when it is not entirely isolated. The shoulder-like structure at the gap borders is also a result of such flawed sp^3-hybridization which reinforces the model predicted in Figure 4b. We have illustrated the charge density plot for the iso-value of 0.1e in Figure 8a and exposed uniform charge distribution at the emission sites of Q-carbon. In this plot, it is evident that the charge density looks like a dumbbell shape (banana type) structure due to the 2p orbital of carbon atoms in the Q-carbon structure which also supports the PDOS results. The three-dimensional (3D) electron density distribution of Q-carbon is calculated by maximizing the entropy (S) under some constraints and the maximum entropy method (MEM) pattern gives valuable information about the electron richness along the Q-carbon emission surface. The MEM pattern is shown in Figure 8b, and it is calculated by[73,74]

$$S = -\sum_{k=1}^{N} \rho_k \ \ln\left(\frac{\rho_k}{\tau_k}\right)$$
(4)

where $\rho_k = \frac{\rho_k^*}{\sum_{k=1}^{N} \rho_k^*}$

The parameters ρ_k and τ_k are the normalized density values from the previous iteration in a 3D gridded space and density obtained from prior information, respectively; N is the total number of pixels in the unit cell. A maximum of 47.45% electron density of carbon is obtained, and it contributes to obtaining the efficient electron field emission characteristics from Q-carbon.

4.3. Work Function Calculation. The work function can be defined as the difference of energy of an electron between the vacuum level and the Fermi level. Mathematically, the work function (φ_w) can be expressed as[75,76]

$$\varphi_w = e\varphi_0 - E_F$$
(5)

Here, φ_0, e, and E_F represent the electrostatic potential of the vacuum level, charge of an electron, and Fermi energy, respectively. We found that the work function of the Q-carbon electron field emitter is around 3.62 eV, which is in good agreement with the previous experimental outcomes.[27] This helps to explain the outstanding field emission characteristics of Q-carbon field emitters. The variation of the electrostatic
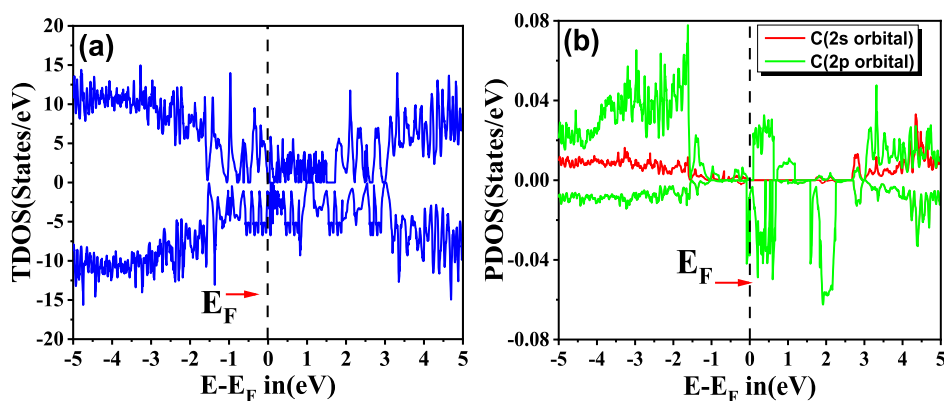
Figure 7. (a) TDOS per eV and (b) PDOS per eV for the Q- carbon structure. (The Fermi levels E_F are shown by black dotted lines in both plots).
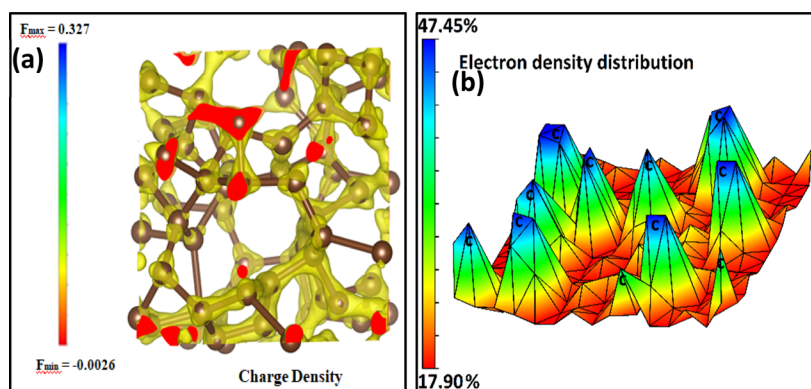

Figure 8. (a) Iso-surface plot for charge density of the amorphous form of Q-carbon for an iso value of 0.1 eV and (b) MEM pattern for electron density distribution. The blue and red regions represent the charge gain and loss, respectively.

potential energy with distance (Å) is shown in Figure 9 for the work function, and the non-zero Fermi level was obtained to be ~2.40 eV.
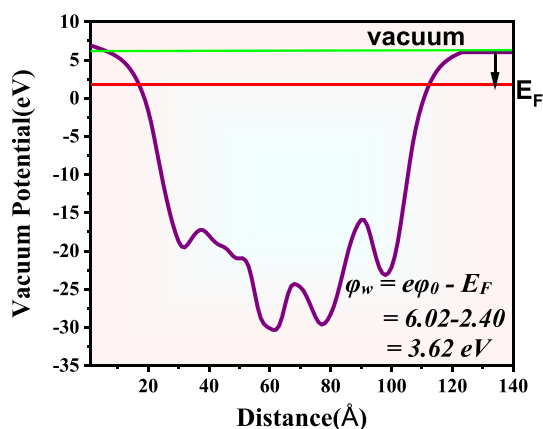

Figure 9. Variation of vacuum potential with distance obtained for the Q-carbon structure used for work function calculation.

5. CONCLUSIONS

In summary, a simple and cost-effective route has been demonstrated for the fabrication of Q-carbon nano-composite thin films with the perspective to observe its exceptional FE performance with the correlation of a DFT study. The homogenous and large-scale Q-carbon nano-composite films were synthesized by PLD and PLA techniques at room

temperature on transparent sapphire substrates, which manifested the features needed for usage in display devices. Very low turn-on electric fields and highly stable electron emissions at high temperatures, up to 500 K, were observed for the Q-carbon field emitters. The F−N linearization and fitting analyses led to the inference of two regimes, and they correspond to distinct field-enhancement factors which change with temperature. The enhanced electron emission originated due to the optimal sp^3/sp^2 ratio, the enhancement in the local electric field caused by the large field-enhancement factors, and the highly stable structure, which is unaffected at high applied electric fields, temperatures, and most importantly during high-density electron emissions. All these factors are responsible for the highly efficient and stable field emission performance. Additionally, the sp^2-bonded carbon atoms with mid-gap states in the sp^3 carbon-rich Q-carbon and the improvement of the spatial conductivity in the surrounding amorphous carbon region due to the sp^2 carbon-rich network are responsible for the exceptional field emission properties. The understanding of the field-emission mechanisms, that take place in such nanostructured Q-carbon composite and/or electrical hetero-geneous systems, undoubtedly advances the field forward. The analysis of the density of states shows that the Q-carbon electron emitting surface is metallic in nature, and it is due to the localized 2p orbital of carbon atoms. We found that the work function of the Q-carbon layer is 3.62 eV which tremendously favors attaining a high field-enhancement factor to facilitate the generation of a robust field emission current density at a low applied electric field. The low turn-on field and high field-enhancement factor of Q-carbon recommends its

potential application as a high-performance next-generation field emitter in field-emission display, future cold cathode-based electronic devices, field-emission microscopes, and so forth.

■ AUTHOR INFORMATION

Corresponding Author

Ariful Haque − *Electrical Engineering, Ingram School of Engineering, Texas State University, San Marcos, Texas 78666, United States; Materials Science, Engineering & Commercialization Program, Texas State University, San Marcos, Texas 78666, United States;* ⓘ orcid.org/0000-0002-4285-9951; Email: ahaque@txstate.edu

Authors

Subrata Karmakar − *Electrical Engineering, Ingram School of Engineering, Texas State University, San Marcos, Texas 78666, United States;* ⓘ orcid.org/0000-0001-7619-5877

Ravi Kumar Trivedi − *High Pressure & Synchroton Radiation Physics Division, Bhabha Atomic Research Centre, Mumbai 400085, India;* ⓘ orcid.org/0000-0002-5964-3401

Brahmananda Chakraborty − *High Pressure & Synchroton Radiation Physics Division, Bhabha Atomic Research Centre, Mumbai 400085, India; Homi Bhabha National Institute, Mumbai 400094, India;* ⓘ orcid.org/0000-0001-9611-099X

Ravi Droopad − *Electrical Engineering, Ingram School of Engineering, Texas State University, San Marcos, Texas 78666, United States; Materials Science, Engineering & Commercialization Program, Texas State University, San Marcos, Texas 78666, United States*

Complete contact information is available at:
https://pubs.acs.org/10.1021/acsomega.2c07576

Notes

The authors declare no competing financial interest.

■ ACKNOWLEDGMENTS

■ REFERENCES

(1) Wang, Q.; Jiang, J. An Overview on Structure and Field Emission Properties of Carbon Nitride Films. *J. Nanomater.* **2014**, *2014*, 1−8.

(2) Davis, R. F. Deposition, Characterization, and Device Development in Diamond, Silicon Carbide, and Gallium Nitride Thin Films. *J. Vac. Sci. Technol. Vac. Surf. Films* **1993**, *11*, 829−837.

(3) Robertson, J. Electron Field Emission from Diamond and Diamond-like Carbon for Field Emission Displays. *Carbon* **1999**, *37*, 759−763.

(4) Zanin, H.; May, P. W.; Hamanaka, M. H. M. O.; Corat, E. J. Field Emission from Hybrid Diamond-like Carbon and Carbon Nanotube Composite Structures. *ACS Appl. Mater. Interfaces* **2013**, *5*, 12238−12243.

(5) Wang, Q. H.; Setlur, A. A.; Lauerhaas, J. M.; Dai, J. Y.; Seelig, E. W.; Chang, R. P. H. A Nanotube-Based Field-Emission Flat Panel Display. *Appl. Phys. Lett.* **1998**, *72*, 2912−2913.

(6) Küttel, O. M.; Groening, O.; Emmenegger, C.; Schlapbach, L. Electron Field Emission from Phase Pure Nanotube Films Grown in a Methane/Hydrogen Plasma. *Appl. Phys. Lett.* **1998**, *73*, 2113−2115.

(7) Hoecker, C.; Smail, F.; Bajada, M.; Pick, M.; Boies, A. Catalyst Nanoparticle Growth Dynamics and Their Influence on Product Morphology in a CVD Process for Continuous Carbon Nanotube Synthesis. *Carbon* **2016**, *96*, 116−124.

(8) Bonard, J.-M.; Salvetat, J.-P.; Stöckli, T.; de Heer, W. A.; Forró, L.; Châtelain, A. Field Emission from Single-Wall Carbon Nanotube Films. *Appl. Phys. Lett.* **1998**, *73*, 918−920.

(9) Liu, H.; Kato, S.; Saito, Y. Effect of Cathode−Anode Distance on Field Emission Properties for Carbon Nanotube Film Emitters. *Jpn. J. Appl. Phys.* **2009**, *48*, 015007.

(10) Tsai, J. T. H.; Chu, T. Y. E.; Shiu, J.-Y.; Yang, C.-S. Field Emission from an Individual Freestanding Graphene Edge. *Small* **2012**, *8*, 3739−3745.

(11) Yamaguchi, H.; Masuzawa, T.; Nozue, S.; Kudo, Y.; Saito, I.; Koe, J.; Kudo, M.; Yamada, T.; Takakuwa, Y.; Okano, K. Electron Emission from Conduction Band of Diamond with Negative Electron Affinity. *Phys. Rev. B: Condens. Matter Mater. Phys.* **2009**, *80*, 165321.

(12) Abubakr, E.; Zkria, A.; Ohmagari, S.; Katamune, Y.; Ikenoue, H.; Yoshitake, T. Laser-Induced Phosphorus-Doped Conductive Layer Formation on Single-Crystal Diamond Surfaces. *ACS Appl. Mater. Interfaces* **2020**, *12*, 57619−57626.

(13) Komlenok, M.; Bolshakov, A.; Ralchenko, V.; Konov, V.; Conte, G.; Girolami, M.; Oliva, P.; Salvatori, S. Diamond Detectors with Laser Induced Surface Graphite Electrodes. *Nucl. Instrum. Methods Phys. Res. Sect. Accel. Spectrometers Detect. Assoc. Equip.* **2016**, *837*, 136−142.

(14) Abubakr, E.; Ohmagari, S.; Zkria, A.; Ikenoue, H.; Yoshitake, T. Laser-Induced Novel Ohmic Contact Formation for Effective Charge Collection in Diamond Detectors. *Mater. Sci. Semicond. Process.* **2022**, *139*, 106370.

(15) Mao, D. S.; Wang, X.; Li, W.; Liu, X. H.; Li, Q.; Xu, J. F.; Okano, K. Electron Field Emission from a Patterned Diamond-like Carbon Flat Thin Film Using a Ti Interfacial Layer. *J. Vac. Sci. Technol. B Microelectron. Nanometer Struct.* **2000**, *18*, 2420.

(16) Musa, I.; Munindrasdasa, D. A. I.; Amaratunga, G. A. J.; Eccleston, W. Ultra-Low-Threshold Field Emission from Conjugated Polymers. *Nature* **1998**, *395*, 362−365.

(17) Gröning, O.; Küttel, O. M.; Emmenegger, Ch.; Gröning, P.; Schlapbach, L. Field Emission Properties of Carbon Nanotubes. *J. Vac. Sci. Technol. B Microelectron. Nanometer Struct.* **2000**, *18*, 665.

(18) Narayan, J.; Bhaumik, A.; Gupta, S.; Haque, A.; Sachan, R. Progress in Q-Carbon and Related Materials with Extraordinary Properties. *Mater. Res. Lett.* **2018**, *6*, 353−364.

(19) Zkria, A.; Gima, H.; Yoshitake, T. Application of Nitrogen-Doped Ultrananocrystalline Diamond/Hydrogenated Amorphous Carbon Composite Films for Ultraviolet Detection. *Appl. Phys. A* **2017**, *123*, 167.

(20) Zkria, A.; Shaban, M.; Abubakr, E.; Yoshitake, T. Impedance Spectroscopy Analysis of N-Type (Nitrogen-Doped) Ultrananocrystalline Diamond/p-Type Si Heterojunction Diodes. *Phys. Scr.* **2020**, *95*, 095803.

(21) van Mourik, T.; Bühl, M.; Gaigeot, M.-P. Density Functional Theory across Chemistry, Physics and Biology. *Philos. Trans. R. Soc. Math. Phys. Eng. Sci.* **20142011**, *372*, 20120488.

(22) Kresse, G.; Hafner, J. Ab Initio Molecular Dynamics for Liquid Metals. *Phys. Rev. B: Condens. Matter Mater. Phys.* **1993**, *47*, 558−561.

(23) Kresse, G.; Hafner, J. Ab Initio Molecular-Dynamics Simulation of the Liquid-Metal−Amorphous-Semiconductor Transition in Germanium. *Phys. Rev. B: Condens. Matter Mater. Phys.* **1994**, *49*, 14251−14269.

(24) Kresse, G.; Furthmüller, J. Efficiency of Ab-Initio Total Energy Calculations for Metals and Semiconductors Using a Plane-Wave Basis Set. *Comput. Mater. Sci.* **1996**, *6*, 15−50.

(25) Kresse, G.; Furthmüller, J. Efficient Iterative Schemes for Ab Initio Total-Energy Calculations Using a Plane-Wave Basis Set. *Phys. Rev. B: Condens. Matter Mater. Phys.* **1996**, *54*, 11169−11186.

(26) Pack, J. D.; Monkhorst, H. J. Special Points for Brillouin-Zone Integrations"—a Reply. *Phys. Rev. B: Condens. Matter Mater. Phys.* **1977**, *16*, 1748−1749.

(27) Haque, A.; Narayan, J. Electron Field Emission from Q-Carbon. *Diam. Relat. Mater.* **2018**, *86*, 71−78.

(28) Lv, S.; Li, Z.; Liao, J.; Wang, G.; Li, M.; Miao, W. Optimizing Field Emission Properties of the Hybrid Structures of Graphene Stretched on Patterned and Size-Controllable SiNWs. *Sci. Rep.* **2015**, *5*, 15035.

(29) Bayliss, K. H.; Latham, R. V. An Analysis of Field-Induced Hot-Electron Emission from Metal-Insulator Microstructures on Broad-Area High-Voltage Electrodes. *Proc. R. Soc. Lond. Math. Phys. Sci.* **1986**, *403*, 285−311.

(30) Patra, S. K.; Mohan Rao, G. Field Emission Current Saturation of Aligned Carbon Nanotube—Effect of Density and Aspect Ratio. *J. Appl. Phys.* **2006**, *100*, 024319.

(31) Choi, J. O. Field Emission Properties of Diamondlike Carbon Films Made by a Novel Laser Evaporation Technique. *J. Vac. Sci. Technol. B Microelectron. Nanometer Struct.* **1998**, *16*, 1199.

(32) Li, R. S.; Xie, E. Q.; Zhou, M.; Zhang, Z. X.; Wang, T.; Lu, B. A. Field Emission Properties of Nitrogen Incorporated DLC Films Prepared by Electrodeposition. *Appl. Surf. Sci.* **2008**, *255*, 2787−2790.

(33) Wan, S.; Wang, L.; Zhang, J.; Xue, Q. Field Emission Properties of DLC and Phosphorus-Doped DLC Films Prepared by Electrochemical Deposition Process. *Appl. Surf. Sci.* **2009**, *255*, 3817−3821.

(34) Wächter, R.; Cordery, A.; Proffitt, S.; Foord, J. S. Influence of Film Deposition Parameters on the Field Emission Properties of Diamond-like Carbon Films. *Diam. Relat. Mater.* **1998**, *7*, 687−691.

(35) Li, J. J.; Zheng, W. T.; Jin, Z. S.; Wang, X.; Bian, H. J.; Gu, G. R.; Zhao, Y. N.; Meng, S. H.; He, X. D.; Han, J. C. Electron Field Emission of Radio Frequency Magnetron Sputtered CN⌈Sub x⌉ Films Annealed at Different Temperatures. *J. Vac. Sci. Technol. B Microelectron. Nanometer Struct.* **2003**, *21*, 2382.

(36) Satyanarayana, B. S.; Hart, A.; Milne, W. I.; Robertson, J. Field Emission from Tetrahedral Amorphous Carbon. *Appl. Phys. Lett.* **1997**, *71*, 1430−1432.

(37) Panwar, O. S.; Khan, M. A.; Satyanarayana, B. S.; Bhattacharyya, R.; Mehta, B. R.; Kumar, S.; Ishpal, R. Effect of High Substrate Bias and Hydrogen and Nitrogen Incorporation on Density of States and Field-Emission Threshold in Tetrahedral Amorphous Carbon Films. *J. Vac. Sci. Technol. B Nanotechnol. Microelectron. Mater. Process. Meas. Phenom.* **2010**, *28*, 411−422.

(38) Panwar, O. S.; Khan, M. A.; Kumar, M.; Shivaprasad, S. M.; Satyanarayana, B. S.; Dixit, P. N.; Bhattacharyya, R.; Khan, M. Y. Effect of High Substrate Bias and Hydrogen and Nitrogen Incorporation on Filtered Cathodic Vacuum Arc Deposited Tetrahedral Amorphous Carbon Films. *Thin Solid Films* **2008**, *516*, 2331−2340.

(39) Umehara, Y.; Murai, S.; Koide, Y.; Murakami, M. Effects of Sp2/Sp3 Bonding Ratios on Field Emission Properties of Diamond-like Carbon Films Grown by Microwave Plasma Chemical Vapor Deposition. *Diam. Relat. Mater.* **2002**, *11*, 1429−1435.

(40) Köck, F. A. M.; Garguilo, J. M.; Nemanich, R. J.; Gupta, S.; Weiner, B. R.; Morell, G. Spatial Distribution of Electron Emission Sites for Sulfur Doped and Intrinsic Nanocrystalline Diamond Films. *Diam. Relat. Mater.* **2003**, *12*, 474−480.

(41) Gupta, S.; Weiner, B. R.; Morell, G. Ex Situ Spectroscopic Ellipsometry and Raman Spectroscopy Investigations of Chemical Vapor Deposited Sulfur Incorporated Nanocrystalline Carbon Thin Films. *J. Appl. Phys.* **2002**, *92*, 5457−5462.

(42) Haque, A.; Narayan, J. Stability of Electron Field Emission in Q-Carbon. *MRS Commun.* **2018**, *8*, 1343−1351.

(43) Chen, C.-F.; Tsai, C.-L.; Lin, C.-L. Electronic Properties of Phosphorus-Doped Triode-Type Diamond Field Emission Arrays. *Mater. Chem. Phys.* **2001**, *72*, 210−213.

(44) Carey, J. D.; Forrest, R. D.; Khan, R. U. A.; Silva, S. R. P. Influence of Sp2 Clusters on the Field Emission Properties of Amorphous Carbon Thin Films. *Appl. Phys. Lett.* **2000**, *77*, 2006−2008.

(45) Carey, J. D.; Forrest, R. D.; Silva, S. R. P. Origin of Electric Field Enhancement in Field Emission from Amorphous Carbon Thin Films. *Appl. Phys. Lett.* **2001**, *78*, 2339−2341.

(46) Naik, K. K.; Khare, R.; Chakravarty, D.; More, M. A.; Thapa, R.; Late, D. J.; Rout, C. S. Field Emission Properties of ZnO Nanosheet Arrays. *Appl. Phys. Lett.* **2014**, *105*, 233101.

(47) Zeng, B.; Xiong, G.; Chen, S.; Jo, S. H.; Wang, W. Z.; Wang, D. Z.; Ren, Z. F. Field Emission of Silicon Nanowires. *Appl. Phys. Lett.* **2006**, *88*, 213108.

(48) Viskadouros, G.; Zak, A.; Stylianakis, M.; Kymakis, E.; Tenne, R.; Stratakis, E. Enhanced Field Emission of WS 2 Nanotubes. *Small* **2014**, *10*, 2398−2403.

(49) Li, E.; Cui, Z.; Dai, Y.; Zhao, D.; Zhao, T. Synthesis and Field Emission Properties of GaN Nanowires. *Appl. Surf. Sci.* **2011**, *257*, 10850 S0169433211011871.

(50) Miyauchi, M.; Tokudome, H.; Toda, Y.; Kamiya, T.; Hosono, H. Electron Field Emission from TiO2 Nanotube Arrays Synthesized by Hydrothermal Reaction. *Appl. Phys. Lett.* **2006**, *89*, 043114.

(51) Nützenadel, C.; Küttel, O. M.; Gröning, O.; Schlapbach, L. Electron Field Emission from Diamond Tips Prepared by Ion Sputtering. *Appl. Phys. Lett.* **1996**, *69*, 2662−2664.

(52) Cho, E. S.; Kwon, S. J.; Yang, H. C.; Uh, H. S.; Kim, Y. H.; Park, B.-G.; Lee, J. D. Fabrication and Characterization of Phosphorus-Implanted Mold-Type Diamond Field-Emitter Arrays. *Thin Solid Films* **2003**, *435*, 324−328.

(53) Wang, S. G.; Zhang, Q.; Yoon, S. F.; Ahn, J.; Zhou, Q.; Wang, Q.; Yang, D. J.; Li, J. Q.; Zhang Shanyong, S. Electron Field Emission Enhancement Effects of Nano-Diamond Films. *Surf. Coat. Technol.* **2003**, *167*, 143−147.

(54) Ikeda, T.; Teii, K. Origin of Low Threshold Field Emission from Nitrogen-Incorporated Nanocrystalline Diamond Films. *Appl. Phys. Lett.* **2009**, *94*, 143102.

(55) Li, L.; Sun, W.; Tian, S.; Xia, X.; Li, J.; Gu, C. Floral-Clustered Few-Layer Graphene Nanosheet Array as High Performance Field Emitter. *Nanoscale* **2012**, *4*, 6383.

(56) Varshney, D.; Venkateswara Rao, C.; Guinel, M. J.-F.; Ishikawa, Y.; Weiner, B. R.; Morell, G. Free Standing Graphene-Diamond Hybrid Films and Their Electron Emission Properties. *J. Appl. Phys.* **2011**, *110*, 044324.

(57) Talapatra, S.; Kar, S.; Pal, S. K.; Vajtai, R.; Ci, L.; Victor, P.; Shaijumon, M. M.; Kaur, S.; Nalamasu, O.; Ajayan, P. M. Direct Growth of Aligned Carbon Nanotubes on Bulk Metals. *Nat. Nanotechnol.* **2006**, *1*, 112−116.

(58) Cui, L.; Chen, J.; Yang, B.; Sun, D.; Jiao, T. RF-PECVD Synthesis of Carbon Nanowalls and Their Field Emission Properties. *Appl. Surf. Sci.* **2015**, *357*, 1−7.

(59) Forbes, R. G. Low-Macroscopic-Field Electron Emission from Carbon Films and Other Electrically Nanostructured Heterogeneous Materials: Hypotheses about Emission Mechanism. *Solid-State Electron.* **2001**, *45*, 779−808.

(60) Collins, M.; Barklie, R. C.; Anguita, J. V.; Carey, J. D.; Silva, S. R. P. Characterisation of Defects in Thin Films of Hydrogenated Amorphous Carbon. *Diam. Relat. Mater.* **2000**, *9*, 781−785.

(61) Khan, R. U. A.; Carey, J. D.; Silva, S. R. P.; Jones, B. J.; Barklie, R. C. Electron Delocalization in Amorphous Carbon by Ion Implantation. *Phys. Rev. B: Condens. Matter Mater. Phys.* **2001**, *63*, 121201.

(62) Silva, S. R. P.; Carey, J. D. Enhancing the Electrical Conduction in Amorphous Carbon and Prospects for Device Applications. *Diam. Relat. Mater.* **2003**, *12*, 151−158.

(63) Yeong, K. S.; Thong, J. T. L. Effects of Adsorbates on the Field Emission Current from Carbon Nanotubes. *Appl. Surf. Sci.* **2004**, *233*, 20−23.

(64) Semet, V.; Binh, V. T.; Vincent, P.; Guillot, D.; Teo, K. B. K.; Chhowalla, M.; Amaratunga, G. A. J.; Milne, W. I.; Legagneux, P.;

Pribat, D. Field Electron Emission from Individual Carbon Nanotubes of a Vertically Aligned Array. *Appl. Phys. Lett.* **2002**, *81*, 343−345.

(65) Carey, J. D. Engineering the next Generation of Large-Area Displays: Prospects and Pitfalls. *Philos. Trans. R. Soc. Lond. Ser. Math. Phys. Eng. Sci.* **2003**, *361*, 2891−2907.

(66) Shimada, S.; Teii, K.; Nakashima, M. Low Threshold Field Emission from Nitrogen-Incorporated Carbon Nanowalls. *Diam. Relat. Mater.* **2010**, *19*, 956−959.

(67) Robertson, J. Mechanism of Electron Field Emission from Diamond and Diamond-like Carbon. *Eleventh International Vacuum Microelectronics Conference. IVMC'98 (Cat. No.98TH8382)*; IEEE: Asheville: NC, USA, 1998; pp 162−163.

(68) Talin, A. A.; Dean, K. A.; Jaskie, J. E. Field Emission Displays: A Critical Review. *Solid-State Electron.* **2001**, *45*, 963−976.

(69) Gröning, O.; Küttel, O. M.; Gröning, P.; Schlapbach, L. Field Emitted Electron Energy Distribution from Nitrogen-Containing Diamondlike Carbon. *Appl. Phys. Lett.* **1997**, *71*, 2253−2255.

(70) Carey, J. D.; Smith, R. C.; Silva, S. R. P. Carbon Based Electronic Materials: Applications in Electron Field Emission. *J. Mater. Sci. Mater. Electron.* **2006**, *17*, 405−412.

(71) Sakai, Y.; Chelikowsky, J. R.; Cohen, M. L. Simulating the Effect of Boron Doping in Superconducting Carbon. *Phys. Rev. B* **2018**, *97*, 054501.

(72) Narayan, J.; Bhaumik, A. Novel Phase of Carbon, Ferromagnetism, and Conversion into Diamond. *J. Appl. Phys.* **2015**, *118*, 215303.

(73) Karmakar, S.; Mistari, C. D.; Parey, V.; Thapa, R.; More, M. A.; Behera, D. Microporous Networks of $NiMn_2O_4$ as a Potent Cathode Material for Electric Field Emission. *J. Phys. Appl. Phys.* **2020**, *53*, 055103.

(74) Karmakar, S.; Gavali, D. S.; Mistari, C. D.; Thapa, R.; More, M. A.; Behera, D.; Haque, A. Low-Temperature Spin-Canted Magnetism and Bipolaron Freezing Electrical Transition in Potential Electron Field Emitter $NdNiO_3$. *ACS Appl. Electron. Mater.* **2022**, *4*, 3134−3146.

(75) Karmakar, S.; Mistari, C. D.; Vaidyanathan, A.; More, M. A.; Chakraborty, B.; Behera, D. Comparison of Electrochemical Response and Electric Field Emission Characteristics of Pristine La2NiO4 and La2NiO4/CNT Composites: Origin of Multi-Functionality with Theoretical Penetration by Density Functional Theory. *Electrochim. Acta* **2021**, *369*, 137676.

(76) Karmakar, S.; Mistari, C. D.; Shajahan, A. S.; More, M. A.; Chakraborty, B.; Behera, D. Enhancement of Pseudocapacitive Behavior, Cyclic Performance, and Field Emission Characteristics of Reduced Graphene Oxide Reinforced $NiGa_2O_4$ Nanostructured Electrode: A First Principles Calculation to Correlate with Experimental Observation. *J. Phys. Chem. C* **2021**, *125*, 7898−7912.